Localization of ultracold atoms in Zeeman lattices with incommensurate spin-orbit coupling

Dmitry A. Zezyulin [1] and Vladimir V. Konotop [2]

[1]*School of Physics and Engineering, ITMO University, St. Petersburg 197101, Russia*
[2]*Departamento de Física and Centro de Física Teórica e Computacional, Faculdade de Ciências,*
Universidade de Lisboa, Campo Grande, Ed. C8, Lisboa 1749-016, Portugal

We consider a particle governed by a one-dimensional Hamiltonian in which artificial periodic spin-orbit coupling and the Zeeman lattice have incommensurate periods. Using the best rational approximations to such a quasiperiodic Hamiltonian, the problem is reduced to a description of spinor states in a superlattice. In the absence of constant Zeeman splitting, the system acquires an additional symmetry, which hinders the localization. However, if the lattices are deep enough, then localized states can appear even for Zeeman field with a zero or small mean value. Spatial distribution of localized modes is nearly uniform and is directly related to the topological properties of the effective superlattice: center-of-mass coordinates of modes are determined by Zak phases computed from the superlattice band structure. The best rational approximations feature the "memory" effect: Each rational approximation holds the information about the energies and spatial distribution of the modes obtained under preceding, less accurate approximations. Dispersion of low-energy initial wave packets is characterized by the law $\propto t^{\beta}$, with β varying between $1/2$ at the initial stage and 1 at longer, but still finite-time, evolution. The dynamics of initial wave packets, exciting mainly localized modes, manifests quantum revivals.

I. INTRODUCTION

Eigenstates of a one-dimensional quantum particle in a potential characterized by two incommensurate spatial periods, i.e., in a quasiperiodic potential, are dominated by (but not limited to) spatially localized and delocalized wave functions that correspond to different regions of the energy spectra separated by a threshold energy usually referred to as a mobility edge (ME) [1]. Over the past four decades, the properties of quasiperiodic potentials have been broadly explored using both the tight-binding approximation, i.e., discrete models (see, e.g., [2–6]), and the spatially continuous Schrödinger equation with incommensurate potentials (see, e.g., [7–13]). The existence of localized and delocalized states can also be observed in two-component systems, like spin-orbit-coupled cold atoms [14] with spinor components loaded in identical quasiperiodic optical lattices [15–17]. It has been established that threshold lattice parameters at which the localization-delocalization transition occurs can be strongly modified by the spin-orbit-coupling (SOC)-induced band flattening [18–20]. Emergent phases induced by uniform SOC in a quasiperiodic tight-binding system on a square lattice have been addressed too [21,22].

A setting with spin-orbit-coupled atoms allows for an essentially novel formulation of the localization problem. First, the SOC itself can be modulated in space [23,24] and, in particular, can be periodic. Second, the components of a spinor describing a spin-orbit-coupled atom can experience different, in particular, out-of-phase, periodic potentials [25] constituting a Zeeman lattice. Even without the SOC modulation, such a lattice affects the dynamics of cold atoms very differently in comparison with conventional optical lattices (see, e.g., [19]). The study of the simultaneous effect of periodic SOC modulation and a Zeeman lattice when both have periods whose relation approaches an incommensurate number is the main goal of the present work. We demonstrate that this system features a number of interesting properties. First, we find that a constant component of the Zeeman splitting plays a prominent and ambivalent role: when it is absent, the system acquires an additional symmetry, which imposes that any localized state must be degenerate and two peaked. As a result, in this case the localization requires deeper lattices than in the case where the Zeeman field has a nonzero mean. At the same time, at large enough constant Zeeman splitting all modes become delocalized. As a result, there exists a parametric region where the most pronounced localization is achieved for intermediate values of the constant Zeeman field. Second, using the best rational approximations to the incommensurate lattices, we reduce the problem to a spinor in a periodic superlattice and uncover the relation between the spatial distribution of localized modes and topological properties of the effective superlattice. Namely, the coordinate of the center of mass (c.m.) of each localized mode is determined by the Zak phase [26] of the respective superlattice miniband. Third, we report the "memory" effect for successive best rational approximations: Each approximation has memory of the preceding, i.e., less accurate, ones. Finally, studying the dynamics of initially localized wave packets, we observe oscillatory behavior, interpreted as a signature of quantum revivals.

This paper is organized as follows. In Sec. II we introduce the model and describe our approach, which relies on the approximation of the quasiperiodic two-component

Hamiltonian with an exactly periodic superlattice. Section III presents numerical results for the localization of the eigenstates of the obtained Hamiltonian. Section IV addresses the dynamics of the system below and above the localization transition. Section V concludes the paper.

II. THE MODEL

A. Best rational approximations and effective Hamiltonians

Let us consider a spin-orbit-coupled atom governed by the dimensionless Hamiltonian as follows:

$$H = \frac{1}{2}[-i\partial_x + a(x)\sigma_1]^2 + \frac{\Lambda + \Omega(x)}{2}\sigma_3. \quad (1)$$

Here $a(x)$ is a real-valued π-periodic function (it will be referred to below as a SOC lattice): $a(x) = a(x + \pi)$, and $\sigma_{1,2,3}$ are the Pauli matrices. The Zeeman field consists of a constant component Λ and a π/κ-periodic lattice: $\Omega(x) = \Omega(x + \pi/\kappa)$, where κ is an irrational number; that is, the periods of the SOC lattice and Zeeman lattice are incommensurate.

Since a real-world atomic system is finite and, without loss of generality, can be centered at $x = 0$, we address the eigenvalue problem on a finite interval considered to be sufficiently large,

$$H\boldsymbol{\psi} = E\boldsymbol{\psi}, \quad x \in [-\ell/2, \ell/2], \quad (2)$$

where ℓ denotes the spatial extent of the system.

For any irrational κ there exists a sequence $\{\kappa^{(N_1)}, \kappa^{(N_2)}, \ldots\}$ of the best rational approximations (BRAs) of gradually improving accuracy (see, e.g., [27]). Here "the best" means that if a fraction $\kappa^{(N)} = M/N$ is one of the BRAs (with M and N being coprime integers), then it approximates κ better than any other rational number with a denominator less than or equal to N. More formally, $\kappa^{(N)} = M/N$ is one the BRAs if for any pair of coprime integers P and Q, such that $M/N \neq P/Q$ and $0 < Q \leqslant N$, one has $|Q\kappa - P| > |N\kappa - M|$. The sequence of BRAs can be constructed from the continued fraction associated with the irrational number κ: truncation of the infinite continued fraction to a finite number of terms yields one of the BRAs. The more terms one keeps in the truncated continued fraction, the better the accuracy of the obtained BRA is.

Let $\kappa^{(N)} = M/N$ be one of the BRAs to κ (hereafter we use the upper index N to refer to the BRA with denominator N; then the numerator M is uniquely defined). Define a $\pi/\kappa^{(N)}$-periodic function $\Omega^{(N)}(x) = \Omega^{(N)}(x + (N/M)\pi)$, obtained from $\Omega(x)$ by the replacement $\kappa \to \kappa^{(N)}$, and introduce the respective Hamiltonian $H^{(N)}$

$$H^{(N)} = \frac{1}{2}[-i\partial_x + a(x)\sigma_1]^2 + \frac{\Lambda + \Omega^{(N)}(x)}{2}\sigma_3. \quad (3)$$

Hamiltonian (3) features a combination of two commensurate lattices, $a(x)$ and $\Omega^{(N)}(x)$, and therefore represents a periodic superlattice with a period equal to $L^{(N)} = \pi N$. Assuming that $\Omega(x)$ is a continuously differentiable function, one can always find a sufficiently accurate BRA in the sense that the difference

$$\omega^{(N)} = \Omega(x) - \Omega^{(N)}(x) = O((\kappa - \kappa^{(N)})x), \quad |x| \leqslant \frac{\ell}{2}, \quad (4)$$
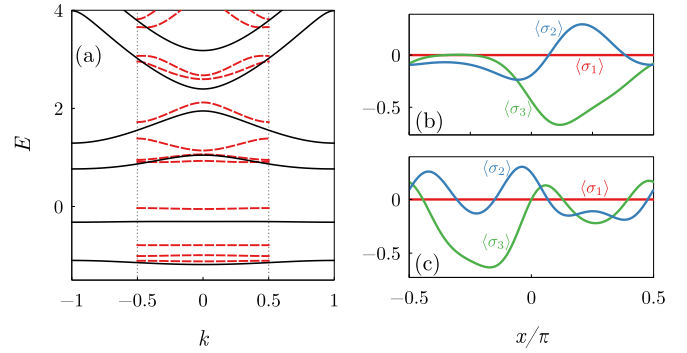

FIG. 1. (a) The lowest energy bands for the π-periodic system with $M = N = 1$ (solid black lines) and 2π-periodic system with $M/N = 3/2$ (dashed red lines) are shown in the respective first Brillouin zones $[-1, 1)$ and $[-1/2, 1/2)$ (the latter shown by vertical dotted lines). Spin densities $\langle\sigma_{1,2,3}\rangle$ computed for the eigenfunctions for (b) the lowest and second-lowest energy bands with $M = N = 1$ at $k = 0$. Here $\Lambda = 3$, $\Omega_0 = 2$, $\alpha = 2$, and $\theta = \pi/3$.

is as small as necessary for $x \in [-\ell/2, \ell/2]$. Thus, any eigenstate of H localized in the interval ℓ can be considered a weakly perturbed state in the Hamiltonian $H^{(N)}$ in the same interval; notice that the above requirement for $\omega^{(N)}$ implies $L^{(N)} \gg \ell$.

Several differences between the introduced system (1) and its approximations (3) and the previously studied discrete models of the Aubry-André (AA) type should be emphasized. Being of spinor character, the Hamiltonian (1) is four-parametric, unlike the two-parametric AA model. With the period of the SOC lattice being fixed, these four parameters are the amplitude of the SOC lattice α [see (17) below], the amplitude of the Zeeman lattice Ω_0, the constant Zeeman splitting Λ, and the phase shift θ between the two lattices. Furthermore, although the incommensurate limit corresponds to the Brillouin zones of the successive approximations shrinking to zero (see the illustration in Fig. 1) and thus to the limit of extremely flat low bands, the tight-binding approximation is not applicable. Indeed, in the incommensurate limit the lattices $a(x)$ and $\Omega(x)$ are not required to be deep enough to justify the tight-binding approximation for several lowest levels. Furthermore, a Zeeman lattice incorporates sublattices for two spinor components with opposite signs: where for one component the potential has a minimum, the potential for the other component has a maximum and vice versa. Thus, the localization of the modes below the ME is not determined by positions of equally spaced deep potential minima; instead, as we show below, the places where modes are situated are determined by the Zak phases, i.e., by the topology of the superlattice.

B. Periodic boundary conditions

To describe the localized states of H, one can consider the eigenvalue problem for $H^{(N)}$ (cf. [8,10]) subject to desirable boundary conditions. Periodicity of $H^{(N)}$ implies that periodic boundary conditions are the most promising choice, whose advantages include the possibility to relate the problem to the Bloch theory and employ topological characteristics of

periodic systems. Therefore, from now on our goal is the study of the localization of atomic states and the evolution of wave packets governed by the approximated Hamiltonian $H^{(N)}$ with the focus on sufficiently large N (formally tending to infinity). More specifically, we consider the eigenvalue problem for $H^{(N)}$,

$$H^{(N)}\boldsymbol{\psi}^{(N)}(x) = E^{(N)}\boldsymbol{\psi}^{(N)}(x), \tag{5}$$

where $\boldsymbol{\psi}^{(N)}(x)$ is a two-component spinor wave function in the interval

$$x \in [-L^{(N)}/2, L^{(N)}/2] =: I^{(N)} \tag{6}$$

subject to periodic boundary conditions,

$$\boldsymbol{\psi}^{(N)}(-L^{(N)}/2) = \boldsymbol{\psi}^{(N)}(L^{(N)}/2), \tag{7}$$

and normalization

$$\int_{I^{(N)}} [\boldsymbol{\psi}^{(N)}(x)]^{\dagger} \boldsymbol{\psi}^{(N)}(x) \, dx = 1. \tag{8}$$

The eigenvalue problem (5) with boundary conditions (7) has a discrete spectrum whose eigenenergies will be denoted by $E_1^{(N)} \leqslant E_2^{(N)} \leqslant \cdots \leqslant E_{\nu}^{(N)} \leqslant \cdots$, where the lower index $\nu = 1, 2, \ldots$ enumerates the eigenenergies and respective eigenvectors $\boldsymbol{\psi}_{\nu}^{(N)}$. Given an eigenstate $\boldsymbol{\psi}_{\nu}^{(N)}$, the quantitative measure of its localization within the interval $I^{(N)}$ can be conveniently represented by the inverse participation ratio (IPR)

$$\chi_{\nu}^{(N)} = \int_{I^{(N)}} \left([\boldsymbol{\psi}_{\nu}^{(N)}]^{\dagger} \boldsymbol{\psi}_{\nu}^{(N)} \right)^2 dx. \tag{9}$$

Large, $\chi_{\nu}^{(N)} \gg 1/L^{(N)}$, and small, $\chi_{\nu}^{(N)} \lesssim 1/L^{(N)}$, values of the IPR correspond to localized and delocalized states.

Under the periodic boundary conditions (7), the position of a localized mode within the superlattice period can be computed as [28]

$$\mathfrak{X}_{\nu}^{(N)} = \frac{L^{(N)}}{2\pi} \arg \left\{ \int_{I^{(N)}} [\boldsymbol{\psi}_{\nu}^{(N)}]^{\dagger} \boldsymbol{\psi}_{\nu}^{(N)} e^{2\pi i x/L^{(N)}} dx \right\}, \tag{10}$$

where the principal value of the argument must be chosen, i.e., $\arg \in (-\pi, \pi]$. Generally speaking, the position defined in (10) is different from the conventional c.m., which is defined as

$$x_{\nu}^{(N)} = \int_{I^{(N)}} x [\boldsymbol{\psi}_{\nu}^{(N)}]^{\dagger} \boldsymbol{\psi}_{\nu}^{(N)} dx \tag{11}$$

and is usually used when localization on the whole real axis is considered. In the meantime, the difference between $\mathfrak{X}_{\nu}^{(N)}$ and $x_{\nu}^{(N)}$ becomes appreciable only for states localized near the boundaries of the interval $I^{(N)}$, i.e., near $x = \pm L^{(N)}/2$. Since we are interested in the limit $N \gg 1$, the relative number of such modes is small, which means that their contribution to the results presented below is negligible. Therefore, we will have $\mathfrak{X}_{\nu}^{(N)} \approx x_{\nu}^{(N)}$ for almost all localized modes.

C. Superlattice band structure and Zak phases

Since the Hamiltonian $H^{(N)}$ admits the periodic continuation from the interval $I^{(N)}$ to the entire real axis, it is natural to explore the band-gap spectrum of the corresponding eigenvalue problem. Considering $x \in \mathbb{R}$, one can formulate the eigenvalue problem as follows: $H^{(N)}\boldsymbol{\varphi}_{\nu k}^{(N)}(x) =$

$\varepsilon_{\nu}^{(N)}(k)\boldsymbol{\varphi}_{\nu k}^{(N)}(x)$. Here $\boldsymbol{\varphi}_{\nu k}^{(N)}(x) = e^{ikx}\boldsymbol{u}_{\nu k}^{(N)}(x)$ are Bloch states, with $\boldsymbol{u}_{\nu k}^{(N)}(x) = \boldsymbol{u}_{\nu k}^{(N)}(x + L^{(N)})$ being $L^{(N)}$-periodic functions, $\varepsilon_{\nu}^{(N)}(k)$ are the energies, index $\nu = 0, 1, \ldots$ enumerates the spectral bands, and the Bloch wave number k runs over the reduced Brillouin zone of the superlattice: $k \in [-1/N, 1/N]$. The usual normalization requires that $\int_{I^{(N)}} [\boldsymbol{u}_{\nu k}^{(N)}]^{\dagger} \boldsymbol{u}_{\nu k}^{(N)} dx = 1$.

If the superlattice spectrum $\varepsilon_{\nu}^{(N)}(k)$ is computed, the eigenvalues and eigenvectors of the eigenvalue problem (5) with periodic boundary conditions (7) can be obtained as $E_{\nu}^{(N)} = \varepsilon_{\nu}^{(N)}(0)$ and $\boldsymbol{\psi}_{\nu}^{(N)}(x) = \boldsymbol{\varphi}_{\nu 0}^{(N)}(x)$. In other words, each solution of (5)–(7) is a Bloch state at $k = 0$ of the effective periodic lattice defined on the whole real axis by the given BRA. Moreover, using the superlattice band structure, the spatial position of localized modes $\boldsymbol{\psi}_{\nu}^{(N)}(x)$ defined in (10) can be estimated from the topology of the corresponding band. Indeed, for each band of the superlattice one can compute the Zak phase [26]

$$\gamma_{\nu}^{(N)} = \int_{-1/N}^{1/N} \Xi_{\nu}^{(N)}(k) dk, \tag{12}$$

where

$$\Xi_{\nu}^{(N)}(k) = i \int_{I^{(N)}} \left[\boldsymbol{u}_{\nu k}^{(N)}(x)\right]^{\dagger} \frac{\partial}{\partial k} \boldsymbol{u}_{\nu k}^{(N)}(x) dx \tag{13}$$

is the Berry connection. In terms of the Wannier functions [29]

$$\boldsymbol{w}_{\nu}^{(N)}(x - \pi m N) = \frac{N}{2} \int_{-1/N}^{1/N} e^{-i\pi k m N} \boldsymbol{\varphi}_{\nu k}^{(N)}(x) dk, \tag{14}$$

the Zak phase can be expressed as

$$\gamma_{\nu}^{(N)} = \frac{2}{N} \int_{-\infty}^{\infty} x [\boldsymbol{w}_{\nu}^{(N)}(x)]^{\dagger} \boldsymbol{w}_{\nu}^{(N)}(x) dx. \tag{15}$$

Those eigenstates which are well localized inside the interval $I^{(N)}$ can be approximated by the Wannier functions computed from the respective superlattice bands, i.e., $\boldsymbol{\psi}_{\nu}^{(N)}(x) \approx \boldsymbol{w}_{\nu}^{(N)}(x)$ for $x \in I^{(N)}$, and therefore, we obtain the relations

$$\mathfrak{X}_{\nu}^{(N)} \approx x_{\nu}^{(N)} \approx \frac{N}{2} \gamma_{\nu}^{(N)}. \tag{16}$$

To conclude this section, we emphasize that while periodic boundary conditions are used and the effective periodic extension of the potential is exploited, the physical applications of the results remain meaningful only inside the interval $I^{(N)}$.

III. NUMERICAL RESULTS

A. Rational approximations

To perform a numerical study, we have chosen the π-periodic SOC lattice in the form

$$a(x) = \alpha \cos(2x), \tag{17}$$

where α is the lattice depth, and the πN-periodic Zeeman lattice

$$\Omega^{(N)}(x) = \Omega_0 \sin \left(2\frac{M}{N}x + \theta\right), \tag{18}$$

where the fraction M/N is one of the BRAs to $\kappa = \sqrt{2}$. The function $\Omega^{(N)}(x)$ is an approximation to $\Omega(x) = \Omega_0 \sin(2\sqrt{2}x + \theta)$ in the quasiperiodic Hamiltonian (1). In the

explicit form, several first BRAs for $\sqrt{2}$ are given as [30]

$$\frac{M}{N} = \frac{1}{1}, \frac{3}{2}, \frac{7}{5}, \frac{17}{12}, \frac{41}{29}, \frac{99}{70}, \frac{239}{169}, \frac{577}{408}, \frac{1393}{985}, \ldots . \quad (19)$$

We emphasize, however, that our analysis, as well as the main conclusions, remains valid for any irrational number. Nowhere in the subsequent analysis is the specificity of the above choice used; only the set of fractions M/N (19) giving the best rational approximation will be modified for another choice of κ. A specific choice of the phase shift between the SOC and Zeeman lattices, i.e., angle θ in (18), also has no significant impact on the results presented below, except for certain particular values of θ at which the system acquires an additional symmetry (see Sec. III E).

Before we proceed with our main results, it is instructive to compare the band structure corresponding to the two least accurate BRAs in (19). For $M/N = 1$ the periods of both lattices are equal to π. In Fig. 1(a) we compare the few lowest energy bands of the resulting π-periodic Hamiltonian with the band structure of the 2π-periodic system obtained for $M/N = 3/2$. We observe the standard splitting of the bands of the π-periodic lattice into the $N = 2$ *minibands*. In Figs. 1(b) and 1(c) we show the distribution of the spin densities $\langle \sigma_j \rangle = \psi^\dagger \sigma_j \psi$ ($j = 1, 2, 3$) at $k = 0$.

Although the eigenvalue problem (5) with the periodic boundary conditions (7) has a purely discrete spectrum $E_\nu^{(N)}$ ($\nu = 1, 2, \ldots$), defining the difference between the adjacent energies, $\Delta_\nu^{(N)} = E_{\nu+1}^{(N)} - E_\nu^{(N)}$, and bearing in mind the periodic continuation described above, one can employ the terminology of periodic potentials, considering "gaps" (relatively large $\Delta_\nu^{(N)}$) and "minigaps" (relatively small $\Delta_\nu^{(N)}$).

Let us choose one of the BRAs from (19), say, $M/N = 239/169$. In view of the variety of the parameters, we first focus on the effect of the increasing constant Zeeman splitting Λ with all other parameters being fixed. For a few different values of Λ we have computed several hundreds of the smallest eigenvalues $E_\nu^{(N)}$. The eigenvalue problem (5)–(7) has been solved numerically using a Floquet-Fourier-Hill-type method [31,32]. In Fig. 2(a) we plot the differences $\Delta_\nu^{(N)}$ for several values of constant Zeeman field Λ. The distinctive pattern that can be observed from this plot indicates that, irrespective of the value of Λ, the gaps are situated between the modes with certain numbers determined by the BRAs (which are discussed in Sec. III C).

B. Localized modes and the mobility edge

Next, we examine the localization, the existence of a ME, and the spatial distribution of localized modes. In Fig. 2(b) we plot the IPR $\chi_\nu^{(N)}$ versus the mode number for several values of the constant Zeeman field Λ. At $\Lambda = 0$, all eigenfunctions are delocalized (with the IPR $\chi_\nu^{(N)}$ not exceeding 0.02, not shown in Fig. 2), which can be partially explained by an additional symmetry that the system acquires at $\Lambda = 0$ (see below in this section). For sufficiently small values of Λ [see $\Lambda = 0.5$ in Fig. 2(b)], the IPR remains small for all eigenfunctions. At larger values of Λ a sharp ME emerges [see $\Lambda = 3$ and 4 in Fig. 2(b)] which separates a fraction of localized modes with lower energies from the rest of the spectrum. Comparing the two panels in Fig. 2, we observe that the location of the
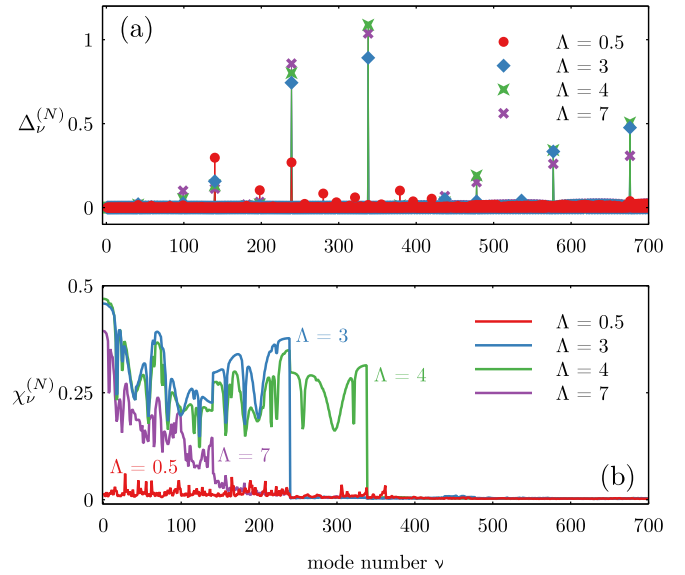

FIG. 2. (a) Difference $\Delta_\nu^{(N)}$ between the adjacent eigenenergies vs the mode number ν for several values of the constant Zeeman splitting Λ. (b) IPR $\chi_\nu^{(N)}$ for the same eigenvalues. Here $N = 169$ ($M/N = 239/169$), $\theta = \pi/3$, $\Omega_0 = 2$, and $\alpha = 2$. For each value of Λ, the corresponding plots are obtained from the 700 smallest eigenvalues.

ME (when the latter exists) coincides with the position of one of the gaps in the discrete spectrum (corroborating previous studies on the one-component Schrödinger equation with quasiperiodic potential [13]). This implies that the chosen BRA determines not only the position of the gaps in the spectrum of eigenenergies but also the number of localized eigenstates. In Fig. 2 this number is equal to 239 and 338 for $\Lambda = 3$ and 4, respectively. In the meantime, the further increase of Λ, formally to the limit $\Lambda \to \infty$, results in the degradation of the sharp ME and in the general decrease in the values of the IPR [see $\Lambda = 7$ in Fig. 2(b)]. This is a manifestation of the Paschen-Back effect, also known as the nonlinear Zeeman effect [33–35] (we notice that delocalization of particles caused by strong random SOC was recently described in [36]). A large Zeeman field Λ results in a strong imbalance between the components (for a large positive Λ one has $|\psi_2| \gg |\psi_1|$), which means that the effect of the SOC lattice becomes essentially perturbative, and the behavior of the system is dominated by the periodic Zeeman lattice, which alone is not sufficient for the localization.

We notice that the dimensionless x is measured in units of λ/π, where λ is the dimensional physical period of the Zeeman lattice, while the lattice amplitude is measured in units of $2E_r$, where $E_r = \hbar^2 \pi^2/(2\lambda^2 m)$ is the recoil energy (m is the atomic mass). Thus, $\Omega_0 = 2$ corresponds to a lattice with amplitude $2E_r$ (i.e., not too deep). The length $N\pi$ corresponds to 500 μm for $N = 169$ and for the physical period of $\lambda = 3 \mu$m.

The fact that all eigenstates shown in Fig. 2 are delocalized for zero and small values of the constant Zeeman field, $\Lambda = 0$, can be, to some extent, explained by analyzing symmetries of the system. We notice that for any Λ both the quasiperiodic Hamiltonian H and its superlattice approximation $H^{(N)}$
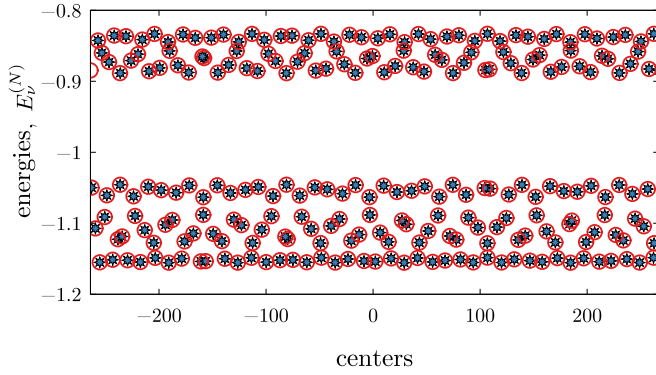
FIG. 3. Centers $\mathfrak{X}_\nu^{(N)}$ (red circles) and $\gamma_\nu^{(N)}N/2$ (blue stars) for all modes with energies below the ME. Here $N = 169$ ($M/N = 239/169$), $\Lambda = 3$, $\theta = \pi/3$, $\Omega_0 = 2$, and $\alpha = 2$. There are 239 localized modes below the ME.

feature a time-reversal symmetry $\sigma_3\mathcal{K}$ ($\mathcal{K}$ is the operator of complex conjugation): $[H, \sigma_3\mathcal{K}] = [H^{(N)}, \sigma_3\mathcal{K}] = 0$, meaning that any nondegenerate state is $\sigma_3\mathcal{K}$ symmetric and thus can be represented in the form $\boldsymbol{\psi} = (\psi_1(x), i\psi_2(x))^T$, where $\psi_{1,2}(x)$ are real. At the same time, for $\Lambda = 0$ the Hamiltonian $H^{(N)}$ with lattices given by (17) and (18) acquires an additional symmetry. Introducing the translation over the half period $T^{(N)} : x \rightarrow x + \pi N/2$, we find that $[H^{(N)}, \sigma_1 T^{(N)}] = 0$ for even N and $[H^{(N)}, \sigma_1 T^{(N)}\mathcal{K}] = 0$ for odd N. This additional symmetry implies that any localized state that exists at $\Lambda = 0$ is generically degenerate and consists of two peaks spatially separated by the half period $L^{(N)}/2$.

At the same time, the half-period translation symmetry does not completely forbid the localization at $\Lambda = 0$: we found that the simultaneous increase of SOC-lattice and Zeeman-lattice depths (starting with approximately $\Omega_0 \gtrsim 4$ and $\alpha \gtrsim 4$) eventually enables the existence of states composed of two localized peaks spatially separated by the half period (more precisely, there are two peaks in each component, ψ_1 and ψ_2, of the spinor eigenstate $\boldsymbol{\psi}$). Localization for a small, but nonzero, Λ is also illustrated in Fig. 5(c) below.

As established above in Eq. (16), the periodic continuation of the superlattice Hamiltonian over the entire real axis provides a connection between the spatial distribution of localized eigenstates and the Zak phases of the bands of the corresponding superlattice. In order to illustrate this observation, in Fig. 3 we compare the values $N\gamma_\nu^{(N)}/2$ computed numerically from the superlattice band spectrum with the centers of localized states obtained directly by substituting the numerically found eigenvectors of (5) into the definition in Eq. (10). The validity of approximation (16) is verified for all localized modes, except for a few states situated at the boundaries of the interval $I^{(N)}$.

C. Memory effect

Figure 3 reveals several other interesting traits. For the chosen parameters, the localized modes are clustered in the two lowest bands, and the centers of modes form a quasiperiodic pattern in each band. The energy distribution of the modes is not uniform within each band: the localized modes tend to accumulate near the energy band edges, revealing an

expectable increase of the density of states near the band edges. At the same time, the distribution of the centers of the localized modes along the interval $I^{(N)}$ is nearly uniform. This suggests an intuitive explanation of the fact that the spectrum computed for the given BRA "remembers" some information about the previous (i.e., less accurate) BRAs. Indeed, let M_1/N_1 and M_2/N_2 be two BRAs with $N_1 < N_2$ (i.e., the second BRA is more accurate). Then the corresponding superlattice period $I^{(N_2)}$ can be represented as $I^{(N_2)} = I_- \cup I^{(N_1)} \cup I_+$, where I_- and I_+ are intervals $[-\pi N_2/2, -\pi N_1/2)$ and $[\pi N_1/2, \pi N_2/2)$, respectively. Both intervals $I^{(N_1)}$ and $I^{(N_2)}$ are uniformly covered by localized states. At the same time, if N_1 and N_2 are large, then the states inside the interval $I^{(N_1)}$ located sufficiently far from its boundaries are weakly affected by the replacement of $\Omega^{(N_1)}(x)$ by $\Omega^{(N_2)}(x)$ because $\delta\Omega(x) = \Omega^{(N_2)}(x) - \Omega^{(N_1)}(x) \sim (\frac{M_2}{N_2} - \frac{M_1}{N_1})\Omega_0 x$ is small enough. In other words, passing from the less accurate BRA to the more accurate one, one does not significantly affect the states localized within $I^{(N_1)}$, i.e., obtained under the less accurate approximation. Notice that $|\delta\Omega(x)|$ is a very small quantity: After a few first approximations, say, for $N_1 = 70$ and $N_2 = 169$, even at the boundaries of $I^{(N_1)}$ one has $\delta\Omega(x) \approx 9 \times 10^{-3}\Omega_0$. Thus, the localized states in the interval $I^{(N_2)}$ can be viewed as the weakly deformed states of the previous approximation in $I^{(N_1)}$ complemented by the "new" states which are located mainly in the intervals $I_\pm$. Since the localized states are uniformly distributed, the number of localized states $n^{(N_{1,2})}$ for BRAs with N_1 and N_2 are interrelated as

$$n^{(N_2)} \approx n^{(N_1)} + n^{(N_1)}\frac{N_2 - N_1}{N_1} = n^{(N_1)}\frac{N_2}{N_1}. \qquad (20)$$

In other words, considering a sequence of BRAs $N_1 < N_2 < N_3 < \cdots$, one obtains a nested structure of $I^{(N)}$ intervals: $I^{(N_1)} \subset I^{(N_2)} \subset I^{(N_3)} \subset \cdots$. The memory that the N_jth approximation has about its N_{j-1}th predecessor consists of the modes located inside $I^{(N_j)}$ and hence inside $I^{(N_{j-1})}$ as well, i.e., of the modes that belong to both intervals. To illustrate this memory effect, in Fig. 4 we juxtapose the energies and centers of localized modes obtained under two subsequent BRAs with $N_1 = 169$ an $N_2 = 408$. In Fig. 4 we observe that within the smaller interval $I^{(169)}$ the centers and energies computed for both BRAs coincide for almost all localized modes, except for a few modes situated near the boundaries of this interval; that is, the more accurate BRA retains the information about the localized modes that exist under the previous BRA.

The memory effect can also be observed from the position of the gaps in the miniband spectra plotted in Fig. 2(a) (for the stationary Schrödinger equation with an incommensurate bichromatic lattice potential, this phenomenon was discussed in [8]). Trying to understand why the largest gaps $\Delta_\nu^{(N)}$ occur exactly at certain positions ν, let us go back to the band structure of the π-periodic lattice [shown in Fig. 1(a)] that corresponds to the least accurate BRA with $N = M = 1$. Passing to a more accurate BRA with $M, N > 1$, each band of the former lattice splits into N minibands [this is illustrated in Fig. 1(a) for $M/N = 3/2$]. It is natural to expect that the emerging minibands are situated close to bands of the original lattice. This anticipation would imply that the largest gaps between the minibands, i.e., the largest values of $\Delta_\nu^{(N)}$ correspond to $\nu = N, 2N, 3N, \ldots$. However, already from Fig. 1(a)
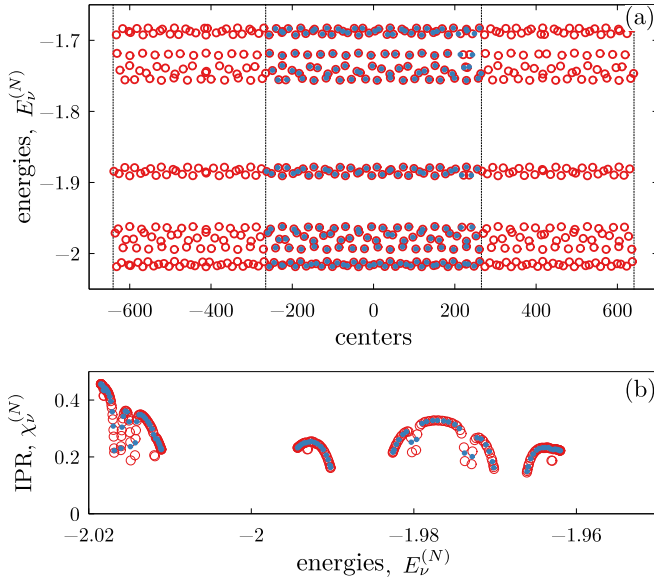
FIG. 4. (a) Centers $\mathfrak{X}_\nu^{(N)}$ for all modes with energies below the ME for two rational approximations: $M/N = 239/169$ (solid blue circles) and $M/N = 577/408$ (open red circles). There are 239 and 577 localized modes below the ME, respectively. Vertical dotted lines correspond to the edges of the intervals $I^{(169)}$ and $I^{(408)}$, $I^{(169)} \subset I^{(408)}$. (b) Dependence of IPR $\chi_\nu^{(N)}$ on energies $E_\nu^{(N)}$ for the two rational approximations. Only the low-energy eigenstates $E_\nu^{(N)} < -1.95$ are shown in this panel. Here $\Lambda = 5$, $\Omega_0 = 2$, $\theta = \pi\sqrt{3}$, and $\alpha = 2$.

it is evident that this first expectation is only partially correct: some of the minibands are situated close to each other even though they emerge from different bands of the original lattice. Nevertheless, the expected pattern still manifests: Analyzing the location of the gaps in Fig. 2(a), we can see that the largest value of $\Delta_\nu^{(N)}$ appears at $\nu = 338$, thus corresponding to $169 + 169$ (i.e., to the chosen $2N$). In the meantime, the second-largest gap in Fig. 2 appears at $\nu = 239$; that is, the relation $239 = 169 + 70$ is verified. Other large gaps are situated at $\nu = 99, 140, 478, 577, 676$. Each of these numbers can be represented as a sum of two (or four) denominators in the sequence (19): $99 = 70 + 29$, $478 = 2(70 + 169)$, $577 = 3 \times 169 + 70$, $676 = 4 \times 169$. Thus, in this picture the positions of the gaps in the discrete spectrum are determined not only by the particular BRA, which is $M/N = 239/169$ in the numerical simulations, but also by the previous BRAs in the series (19). In other words, the spectrum obtained for some particular BRA preserves certain information about the previous, less accurate approximations in the series (19).

D. Global picture

The above study focused on isolated values of the constant Zeeman splitting Λ. Now we fulfill a more thorough examination of the eigenspectrum of problem (5) scanning a finite interval of Λ. In Fig. 5(a) we plot the computed points $(\Lambda, E_\nu^{(N)})$. The pseudocolor represents the value of the IPR for each computed eigenvector. The obtained general picture agrees with the previous considerations. Namely, we observe that for small and large values of Λ the spectrum is poorly localized, i.e., characterized by relatively small
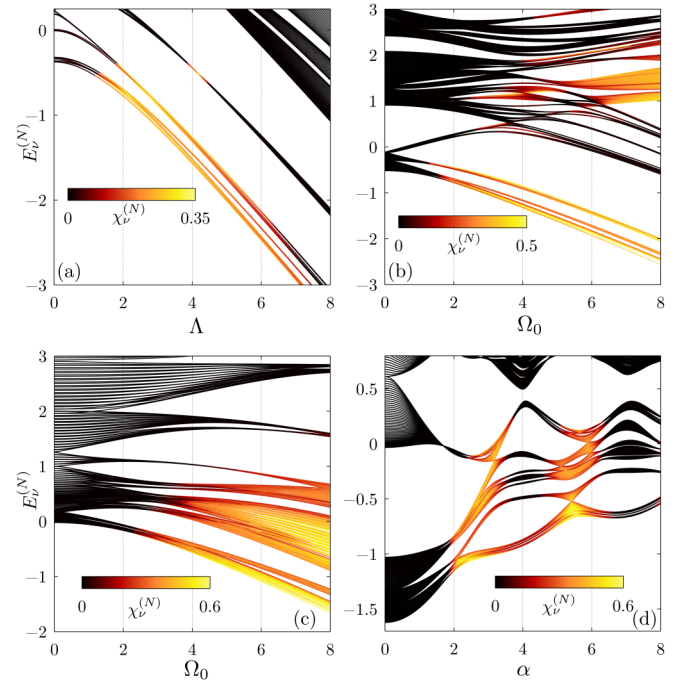

FIG. 5. Pseudocolor plot of IPR vs (a) the amplitude of the constant Zeeman splitting Λ, (b) and (c) the amplitude of the Zeeman lattice Ω_0, and (d) the amplitude of the SOC lattice α. Other parameters are chosen as $\alpha = 2$, $\Omega_0 = 2$ in (a), $\alpha = 2$, $\Lambda = 2$ in (b), $\alpha = 4$, $\Lambda = 0.1$ in (c), and $\Lambda = 3$, $\Omega_0 = 2$ in (d). All panels are obtained for $\theta = \pi/3$, and $M/N = 239/169$ in (a), (b), and (d) and $M/N = 99/70$ in (c).

IPRs corresponding to wave-packet widths comparable to the size of the system $L^{(N)}$. A sharp ME, i.e., one separating energies of delocalized states and the states whose localization domain is much lower than the size of the system, exists for $2 \lesssim \Lambda \lesssim 6$. The location of the ME coincides with the upper edge of the higher band in which the states are localized.

In Fig. 5(b) we show a pseudocolor diagram obtained for a situation in which the value of the constant Zeeman field Λ is fixed but the amplitude of the Zeeman lattice Ω_0 increases gradually from zero. As one can expect, all states are delocalized in a Zeeman lattice with zero and small amplitudes ($\Omega_0 \lesssim 2$). The localization of states from the lowest gaps is gradually enhanced with the increase of Ω_0. Moreover, for sufficiently large Ω_0, one observes several MEs emerging between the groups of energies associated with localized and delocalized eigenstates. In this last case clusters of localized states have energies bigger than those of delocalized states [in Fig. 5(b) this is clearly seen for $\Omega_0 \gtrsim 6$].

In Fig. 5(c) we illustrate the possibility of localization in the Zeeman field with the small mean value $\Lambda = 0.1$. We observe that in this case the localization is also possible but requires the presence of deeper lattices compared to the localization under intermediate values of Λ [compare the values of α and Ω_0 in Figs. 5(a) and 5(c)]. Finally, in Fig. 5(d) we present the localization diagram for the increasing SOC lattice amplitude α. Localization is observed only for a finite interval of the SOC strength and is characterized by the inhomogeneous dependence of the ME on α: For the parameters in

Fig. 5(d) the localization domain is $2 \lesssim \alpha \lesssim 6.5$, while the ME is much lower for the central part of this interval.

E. Degenerate modes

In the generic situation the spectrum in (5) is nondegenerate, i.e., $E_\nu^{(N)} < E_{\nu+1}^{(N)}$ for all (or almost all) ν. However, for special values of the phase shift θ [see Eq. (18)] between the SOC and Zeeman lattices, certain BRAs may enable additional symmetries that result in degeneracies, i.e., in a large number of double eigenenergies $E_\nu^{(N)} = E_{\nu+1}^{(N)}$ emerging in the spectrum. To look for an additional symmetry, let us consider a phase shift of the form $\theta = Q_1 \pi / Q_2$, where $Q_{1,2}$ are coprime integers. Then we can observe that the transformation $x \to P\pi/2 - x$, where integer P satisfies the condition

$$2\frac{Q_1}{Q_2} + P\frac{M}{N} = \text{odd integer}, \tag{21}$$

transforms the superlattice Hamiltonian $H^{(N)}$ with the SOC and Zeeman lattices given by (17) and (18) either to itself (if P is odd) or to its complex conjugate (if P is even). If $\boldsymbol{\psi}_\nu^{(N)}(x)$ is an eigenvector corresponding to the energy $E_\nu^{(N)}$, then, depending on the parity of P, $\boldsymbol{\psi}_\nu^{(N)}(P\pi/2 - x)$ or $\mathcal{K}\boldsymbol{\psi}_\nu^{(N)}(P\pi/2 - x)$ is also an eigenstate corresponding to the same eigenenergy $E_\nu^{(N)}$. If the original and transformed eigenvectors are linearly independent (which is true for most of the modes), then $E_\nu = E_{\nu+1}$ is a double eigenvalue which has a two-dimensional invariant subspace spanned by the found eigenvectors.

Considering (21) as an equation for an unknown P with Q_1/Q_2 and M/N being fixed, we observe that this equation does not always have a solution. For example, for $Q_1/Q_2 = 1/3$ (this is the case considered above) the BRA $M/N = 239/169$ does not allow for an integer solution P. However, for the next BRA from the sequence (19), i.e., for $M/N = 577/408$, one finds a solution $P = 136$. Thus, different BRAs can be "nonequivalent" with respect to this spontaneous symmetry. In the case when the symmetry is present, we have verified numerically that a large number of double eigenenergies $E_\nu^{(N)} = E_{\nu+1}^{(N)}$ emerge in the spectrum. Each double eigenvalue is associated with a two-peaked eigenvector, and the distance between the two peaks is equal to $P\pi/2$.

IV. DYNAMICS

Finally, we briefly discuss the evolution of a time-dependent spinor $\boldsymbol{\Psi}(x,t)$ described by the Schrödinger equation $i\boldsymbol{\Psi}_t(x,t) = H^{(N)}\boldsymbol{\Psi}(x,t)$ considered subject to the periodic boundary conditions (7). Aiming at a qualitative preliminary study, here we present several explicit simulations of the dynamics which illustrate the effect that the presence of localized modes has on the temporal dynamics. The time-dependent equation has been integrated with the $\sigma_3\mathcal{K}$-symmetric initial condition $\boldsymbol{\Psi}(x,t=0) = (1,i)^T \Psi(x)$, where $\Psi(x)$ is a real-valued Gaussian wave packet [the IPR of the initial pulse was $\chi(t=0) = 0.2$]. Since the localized modes are distributed uniformly on the interval $I^{(N)}$, the qualitative dynamics does not depend significantly on the position of the initial wave packet. We created the initial state at the center
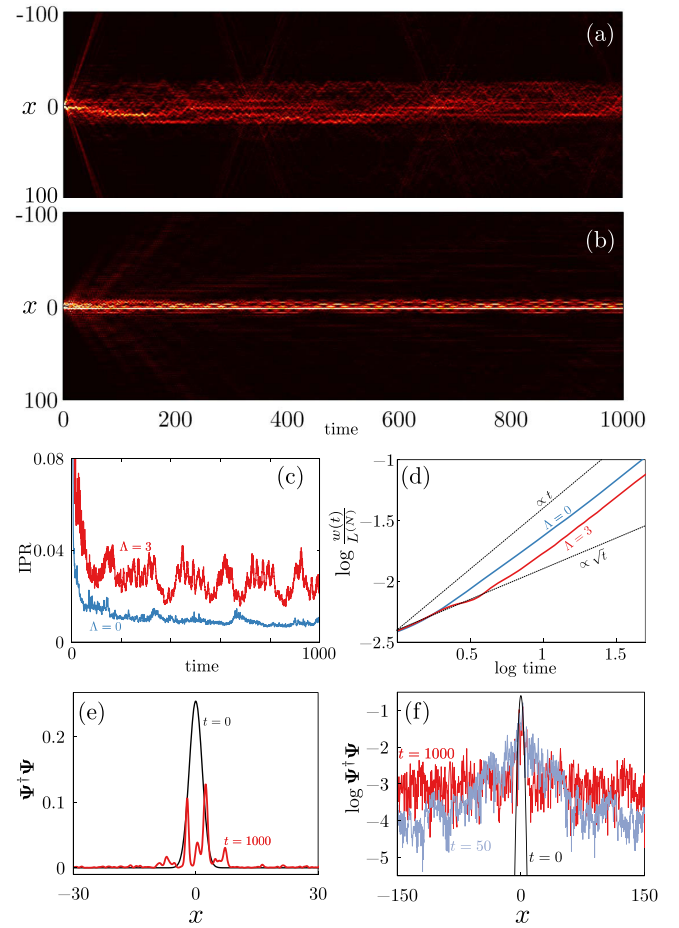

FIG. 6. (a) and (b) Pseudocolor plots of the temporal evolution $\boldsymbol{\Psi}^\dagger\boldsymbol{\Psi}$ below and above the delocalization-localization transition [$\Lambda = 0$ and $\Lambda = 3$ in (a) and (b), respectively]. Only the central part, $x \in [-100, 100]$, of the entire interval $I^{(N)}$ is shown in the plots. (c) The corresponding evolution of the IPR $\chi(t)$. (d) A log-log plot of the widths in units of the full superlattice period $L^{(N)} = \pi N$, plotted for $t \in (0, 50)$. Black dashed lines correspond to the square-root ($\propto \sqrt{t}$) and linear ($\propto t$) laws. (e) and (f) show $\boldsymbol{\Psi}^\dagger\boldsymbol{\Psi}$ at $\Lambda = 3$ and different moments of time t in linear and log scales. Here $M/N = 239/169$, $\Omega_0 = 2$, $\alpha = 2$, and $\theta = \pi/3$.

of the interval $I^{(N)}$. The numerical solution $\boldsymbol{\Psi}(x,t)$ was then used to find the time-dependent IPR $\chi(t)$ and the mean width.

In the presence of localized states, the initial wave packet excites those situated along the width of the distribution $\Psi(x)$, leading to a nondispersing part of the wave packet. Additionally, higher-energy extended sates are excited, which results in partial dispersion. The qualitatively different dynamics in the extended and localized phases are illustrated in Figs. 6(a) and 6(b). Comparing the pseudocolor plots of $\boldsymbol{\Psi}^\dagger\boldsymbol{\Psi}$, we observe that in the case when the localized modes are present in the spectrum, the atom is dominantly localized in the central region [Fig. 6(b)]. Meanwhile, even in the absence of localized states, the dispersion of the wave packet is slowed down by the quasiperiodicity [Fig. 6(a)]. For the characterization of the evolution of the localized modes the time-dependent IPR appears to be the most appropriate quantity [exemplified in Fig. 6(c)], while dispersive spreading at early stages of the

dynamics is more adequately described by the mean-square width of the wave packet $w(t) = \{\int_{I^{(N)}} [x - x_0(t)]^2 \mathbf{\Psi}^\dagger \mathbf{\Psi} dx\}^{1/2}$, where $x_0(t) = \int_{I^{(N)}} x \mathbf{\Psi}^\dagger \mathbf{\Psi} dx$, as shown in Fig. 6(d). In the presence of localized modes, the time evolution of the IPR reveals relatively strong oscillations [see the red line in Fig. 6(c), which shows a superposition of fast and slow oscillations of $\chi(t)$]. Taking into account that the distribution of energies of localized states is nonuniform, the oscillations can be viewed as a manifestation of quantum revivals, typical of a trapped quantum particle.

Figure 6(d) shows the log-log plot for the short-time evolution of the mean width $w(t)$ of the solutions. We observe the $w(t) \propto t^\beta$ law, with β varying between $\beta = 1/2$ at the beginning of the evolution and $\beta = 1$ at larger times [see the dashed lines in Fig. 6 (d)]. It should be mentioned that the exponent β in the nontrivial t^β dependence is likely to be related to the fractal spectrum of the quasiperiodic Hamiltonian (1), as suggested by earlier studies [37] (the investigation of such a relation, however, is left for future investigation).

The atomic density distribution at $t = 1000$ is illustrated in Fig. 6(e). Although the initial shape of the cloud at $t = 1000$ is strongly modified, the localization domain remains nearly the same as that at $t = 0$. This is also confirmed in the logarithmic plot in Fig. 6(f), where we also show the intermediate distribution at $t = 50$, when the spreading wave packet still does not attain the boundaries of the spatial domain $L^{(N)}$ used in the numerics. We verify that while the boundaries do affect the decay of the wave-packet tails, they do not have a significant impact on the atomic cloud distribution in the localization region located in the center of the interval $L^{(N)}$, even at sufficiently large times.

V. CONCLUSION

In this paper, we have considered the properties of the atomic spinor under the effect of a lattice with incommensurate periodic spin-orbit coupling and a Zeeman lattice. When the constant Zeeman splitting is zero, the system acquires an additional symmetry which constraints the shape of the eigenfunctions and therefore inhibits the localization, i.e.,

requires stronger lattice depths for the localization to occur. At sufficiently large constant Zeeman field all modes become delocalized, thus manifesting the well-known Paschen-Back effect. Using the best rational approximations, the consideration of the quasiperiodic Hamiltonian has been reduced to an effective periodic superlattice. When the mobility edge exists, the exact number of localized eigenstates is determined by the chosen rational approximation. Moreover, considering best rational approximations with different accuracies, we found that the more accurate approximation preserves certain information about the rougher one, which we interpreted as a memory effect. Furthermore, spatial positions of localized eigenmodes can be obtained from the Zak phases of minibands of the effective superlattice, revealing the relation between the distribution of the modes in the space and the topology of the effective superlattice. In the presence of localized modes, simulations of the evolution of initially localized wave packets reveal the signature of quantum revivals.

The obtained results are directly applicable to noninteracting spin-orbit-coupled Bose-Einstein condensates. It may therefore be relevant to extend the present study to condensates with nonzero interatomic interactions, which is expected to further enrich the host of features resulting from the combination of the two incommensurate lattices.

We finally mention that, while the presented results for temporal simulations uncovered a qualitatively different wave-packet dynamics in the extended and localized phases, a comprehensive and accurate description of different stages of long-time dynamics requires a separate thorough study.

[1] N. Mott, The mobility edge since 1967, J. Phys. C **20**, 3075 (1987).

[2] S. Aubry and G. André, Analyticity breaking and Anderson localization in incommensurate lattices, Ann. Isr. Phys. Soc. **3**, 133 (1980).

[3] C. M. Soukoulis and E. N. Economou, Localization in One-Dimensional Lattices in the Presence of Incommensurate Potentials, Phys. Rev. Lett. **48**, 1043 (1982).

[4] M. Kohmoto, Metal-Insulator Transition and Scaling for Incommensurate Systems, Phys. Rev. Lett. **51**, 1198 (1983).

[5] D. R. Grempel, S. Fishman, and R. E. Prange, Localization in an Incommensurate Potential: An Exactly Solvable Model, Phys. Rev. Lett. **49**, 833 (1982).

[6] D. J. Thouless, Bandwidths for a quasiperiodic tight-binding model, Phys. Rev. B **28**, 4272 (1983).

[7] M. Ya. Azbel, Quantum Particle in One-Dimensional Potentials with Incommensurate Periods, Phys. Rev. Lett. **43**, 1954 (1979).

[8] R. B. Diener, G. A. Georgakis, J. Zhong, M. Raizen, and Q. Niu, Transition between extended and localized states in a one-dimensional incommensurate optical lattice, Phys. Rev. A **64**, 033416 (2001).

[9] D. J. Boers, B. Goedeke, D. Hinrichs, and M. Holthaus, Mobility edges in bichromatic optical lattices, Phys. Rev. A **75**, 063404 (2007).

[10] M. Modugno, Exponential localization in one-dimensional quasi-periodic optical lattices, New J. Phys. **11**, 033023 (2009).

[11] J. Biddle, B. Wang, D. J. Priour, and S. Das Sarma, Localization in one-dimensional incommensurate lattices beyond the Aubry-André model, Phys. Rev. A **80**, 021603(R) (2009).

[12] X. Li, X. Li, and S. Das Sarma, Mobility edges in one-dimensional bichromatic incommensurate potentials, Phys. Rev. B **96**, 085119 (2017).

[13] H. Yao, H. Khoudli, L. Bresque, and L. Sanchez-Palencia, Critical Behavior and Fractality in Shallow One-Dimensional Quasiperiodic Potentials, Phys. Rev. Lett. **123**, 070405 (2019).

[14] V. Galitski and I. B. Spielman, Spin-orbit coupling in quantum gases, Nature (London) **494**, 49 (2013).

[15] L. Zhou, H. Pu, and W. Zhang, Anderson localization of cold atomic gases with effective spin-orbit interaction in a quasiperiodic optical lattice, Phys. Rev. A **87**, 023625 (2013).

[16] Y. Cheng, G. Tang, and S. K. Adhikari, Localization of a spin-orbit-coupled Bose-Einstein condensate in a bichromatic optical lattice, Phys. Rev. A **89**, 063602 (2014).

[17] C. Li, F. Ye, Y. V. Kartashov, V. V. Konotop, and X. Chen, Localization-delocalization transition in spin-orbit-coupled Bose-Einstein condensate, Sci. Rep. **6**, 31700 (2016).

[18] Y. Zhang and C. Zhang, Bose-Einstein condensates in spin-orbit-coupled optical lattices: Flat bands and superfluidity, Phys. Rev. A **87**, 023611 (2013).

[19] Y. V. Kartashov, V. V. Konotop, D. A. Zezyulin, and L. Torner, Bloch Oscillations in Optical and Zeeman Lattices in the Presence of Spin-Orbit Coupling, Phys. Rev. Lett. **117**, 215301 (2016); Dynamic localization in optical and Zeeman lattices in the presence of spin-orbit coupling, Phys. Rev. A **94**, 063606 (2016).

[20] F. Kh. Abdullaev and M. Salerno, Flat bands and dynamical localization of spin-orbit-coupled Bose-Einstein condensates, Phys. Rev. A **98**, 053606 (2018).

[21] M. Kohmoto and D. Tobe, Localization problem in a quasiperiodic system with spin-orbit interaction, Phys. Rev. B **77**, 134204 (2008).

[22] D. K. Sahu, A. P. Acharya, D. Choudhuri, and S. Datta, Self-duality of one-dimensional quasicrystals with spin-orbit interaction, Phys. Rev. B **104**, 054202 (2021).

[23] K. Jiménez-García, L. J. LeBlanc, R. A. Williams, M. C. Beeler, C. Qu, M. Gong, C. Zhang, and I. B. Spielman, Tunable Spin-Orbit Coupling via Strong Driving in Ultracold-Atom Systems, Phys. Rev. Lett. **114**, 125301 (2015).

[24] X. Luo, L. Wu, J. Chen, Q. Guan, K. Gao, Z.-F. Xu, L. You, and R. Wang. Tunable atomic spin-orbit coupling synthesized with a modulating gradient magnetic field, Sci. Rep. **6**, 18983 (2016).

[25] K. Jiménez-García, L. J. LeBlanc, R. A. Williams, M. C. Beeler, A. R. Perry, and I. B. Spielman, Peierls Substitution in an Engineered Lattice Potential, Phys. Rev. Lett. **108**, 225303 (2012).

[26] J. Zak, Berry's Phase for Energy Bands in Solids, Phys. Rev. Lett. **62**, 2747 (1989).

[27] A. Ya. Khinchin, *Continued Fractions* (University of Chicago Press, Chicago, 1964).

[28] R. Resta, Quantum-Mechanical Position Operator in Extended Systems, Phys. Rev. Lett. **80**, 1800 (1998).

[29] W. Kohn, Analytic properties of Bloch waves and Wannier functions, Phys. Rev. **115**, 809 (1959).

[30] T. Koshy, *Pell and Pell-Lucas Numbers with Applications* (Springer, New York, 2014).

[31] B. Deconinck and J. N. Kutz, Computing spectra of linear operators using the Floquet-Fourier-Hill method, J. Comput. Phys. **219**, 296 (2006).

[32] J. Yang, *Nonlinear Waves in Integrable and Nonintegrable Systems* (Society for Industrial and Applied Mathematics, Philadelphia, 2010).

[33] F. Paschen and E. Back, Normale und anomale Zeemaneffekte, Ann. Phys. (Berlin, Ger.) **344**, 897 (1912); Normale und anomale Zeemaneffekte. Nachtrag, **345**, 960 (1913).

[34] L. D. Landau and E. M. Lifshitz, *Quantum Mechanics* (Butterworth-Heinemann, Oxford, 1981).

[35] B. H. Bransden and C. J. Joachain, *Physics of Atoms and Molecules* (Longman, New York, 1982).

[36] M. Modugno, E. Ya. Sherman, and V. V. Konotop, Macroscopic random Paschen-Back effect in ultracold atomic gases, Phys. Rev. A **95**, 063620 (2017).

[37] R. Ketzmerick, K. Kruse, S. Kraut, and T. Geisel, What Determines the Spreading of a Wave Packet? Phys. Rev. Lett. **79**, 1959 (1997).